Water Resources Management
https://doi.org/10.1007/s11269-025-04161-2

Desilting Efficiency Assessment Under Four Hydraulic Sediment Prevention Operations

Fong-Zuo Lee[1] · **Yu-Yun Du**[1]

Received: 3 September 2024 / Accepted: 26 February 2025

Abstract
Effective sediment management is essential for preserving reservoir storage capacity, water quality, and operational efficiency. Sediment accumulation shortens reservoir lifespan and impacts downstream ecosystems, highlighting the need for optimized hydraulic sediment prevention strategies. This study develops and validates a two-dimensional reservoir model to simulate turbidity currents, sediment transport, and sediment outflow trends, offering valuable insights into sediment management. The study uses field observations and physical model tests to evaluate model performance and use the model to assess four hydraulic sediment prevention operations. Results indicate that downstream replenishment flushing is the most effective sediment removal method, while midstream desilting tunnels significantly reduce transport time. In contrast, the absence of sediment prevention prolongs transport. The desilting tunnel demonstrates the highest sediment removal efficiency, followed by sluicing and flood reduction operations. Immediate tunnel opening and optimal outflow rates further enhance sediment removal. Despite reservoir dilution, peak concentration ratios remain similar across conditions. High-flow scenarios benefit most from timely tunnel activation and sufficient discharge rates, optimizing sediment management. These findings provide insights for optimizing reservoir operations' sediment and water resource management.

Keywords Hydraulic sediment prevention · Desilting tunnel · Downstream replenishment flushing · Water resources management

✉ Fong-Zuo Lee
fzlee@nchu.edu.tw

Yu-Yun Du
leaf71221@gmail.com

[1] Department of Civil Engineering, National Chung Hsing University, 145 Xingda Rd., South Dist, 402202 Taichung City, Taiwan (R.O.C.)

Published online: 08 March 2025

1 Introduction

Reservoir sedimentation can reduce storage capacity and increase the risk of blocking intake structures, threatening the operation of bottom outlets such as those for hydropower plants, public water supplies, and irrigation canals (Morris and Fan 2010). Management strategies to address reservoir sedimentation include techniques such as reducing sediment inflow from the upstream watershed, routing sediment through the reservoir to minimize deposition, and removing sediment deposits (Morris and Fan 2010; Lee et al. 2014; Annandale et al. 2016; Zulfan et al. 2023; Huang 2024). Researchers need to devise better and more effective strategies to combat the inflow of turbid water and significantly minimize deposition during flood events. Additionally, recent studies have explored innovative sediment management strategies, including optimization models for sediment evacuation and sediment redistribution mechanisms in mountain reservoirs (Afzalsoltani and Yazdi 2023; Li and Pasternack 2022).

During flood events, turbidity currents may be generated in reservoirs. These are gravity-driven movements of sediment-laden flows over, through, or under the ambient fluid caused by the density difference between the two fluids (Sastre et al. 2010). Turbidity currents, a density current caused primarily by turbidity, can significantly impact reservoir sediment deposition. Therefore, understanding and analyzing turbidity currents are crucial for sustainable and effective management and operation of hydraulic infrastructure. To avoid sedimentation in critical reservoir locations, it is essential to understand the factors affecting turbidity currents and reservoir sedimentation mitigation. Over the past decade, turbidity flows have been a topic of theoretical debate (Schleiss et al. 2016).

Some studies have focused on current turbidity venting through reservoir outlets and the factors influencing it. For optimum sediment venting, the outlet's location is vital; sediment outflow concentration from bottom outlets is higher than from elevated outlets due to the stratification phenomenon of turbidity currents (Morris and Fan 2010; Lee et al. 2014). Additionally, understanding the timing of gate openings at these reservoir outlets is essential. Chamoun et al. (2018) found that gates should be opened when the turbidity current is approximately 300 m upstream of the outlet to maximize sediment outflow concentration. The bed slope also influences the venting of turbidity currents, with higher venting efficiencies attained when the thalweg upstream of the dam is steeper (Chamoun et al. 2017; Morris and Fan 2010). Furthermore, studies on sediment flushing operations emphasize the importance of hydraulic flushing techniques and pressure-controlled sluicing for improving sediment removal efficiency (Castro and Mantilla 2021; Kalita 2020).

However, observing and analyzing turbidity currents in the field is highly challenging, as they are typically generated during floods, limiting field observation and investigation. Hence, simulating sediment movement in reservoirs using numerical models is crucial for understanding turbidity currents. Hydrodynamic and sediment transport modeling are essential for analyzing sedimentation processes in reservoirs. Numerical models generally employ two-dimensional (2D) or three-dimensional (3D) equations to study sediment-laden flow. While these models can provide accurate predictions for many applications, they need precise calibration.

In regions where three-dimensional effects are significant, such as areas with strong vertical non-uniformity in the flow field, it is necessary to use numerical models based on solving the 3D Navier-Stokes equations, which govern complex fluid flows and sediment concentrations. However, some developed vertical 2D models, such as the CE-QUAL-W2 hydrodynamic model, are also applied to lentic environments to analyze eutrophication, water quality, thermal stratification, and nutrient dynamics in reservoirs (Benicio et al. 2024; Ziaie et al. 2019), as they simplify calculations while considering vertical variations. Among the 3D numerical models, solvers like the CFX series have been used to compute two-phase flow parameters associated with turbidity currents (De Cesare et al. 2001, 2006; Oehy and Schleiss 2007; Lee et al. 2014; Amini et al. 2017; Jodeau et al. 2018; Imtiyaz et al. 2024). However, 3D simulations are much more time-consuming than 2D models, even with GPUs for 3D turbidity current simulations. Therefore, 2D models are relatively efficient and suitable for assessing the sluicing efficiency of bottom outlets under varied hydraulic desiltation operations in reservoirs.

Huang et al. (2019) demonstrated that a 2D model could effectively predict turbidity currents' movement toward dam sites and the sluicing of outlets at various elevations, making it practical for field applications. The study also established guidelines for selecting appropriate sensitivity parameters, emphasizing mesh size and drag coefficient as crucial factors. Anari et al. (2020) confirmed the 2D model's suitability for simulating the horizontal movement of turbidity currents, particularly near reservoir sluice gates, underscoring sediment transportation's importance in maintaining storage sustainability in reservoir management. Chen's (2020) research on the Zengwen Reservoir showcased the 2D model's utility in simulating sediment concentration and desilting efficiency for bottom dredged channels. Wang et al. (2020) proposed a strategy using 2D model simulations that involves compartmentalizing the reservoir, significantly enhancing flushing efficiency depending on specific scenarios, such as partition desilting, empty flushing, or a hybrid approach. They also indicated that creating a narrower, gorge-like geometry could improve desilting efficiency. Further, Hung et al. (2022)nnnnnnn applied a 2D turbidity currents model to simulate sediment concentration distribution and the outflow discharge process in a reservoir area. Lastly, a 2D numerical model to analyze sedimentation mitigation in the Agongdian Reservoir, highlighting its value in assessing the sluicing efficiency of bottom outlets under varied hydraulic desiltation operations (Lee et al. 2023; Lee and Huynh Nguyen 2024) used. Above all, a 2D numerical model is a proper tool for studying turbidity current behavior, including the flow pattern, sediment concentration, and releasing amount. Therefore, this study adapts a 2D numerical model to assess Desilting efficiency under four hydraulic sediment prevention operations.

2 Methods

2.1 Study Site

Nanhua Reservoir is located in Nanhua District, Tainan City, Taiwan, upstream of the Houku River, a tributary of the Zengwen River. The reservoir was completed in 1993, and its water source came from the Houku River and Jiasian Weir, tributaries of the Gaoping River. The watershed area of Nanhua Reservoir is 108.30 km (Amini et al. 2017), and its scope and location are shown in Fig. 1. Its designed water capacity is 150 million m (Anari et al. 2020). Nanhua Reservoir has four main facilities: the dam, spillway, water intake, and Desilting tunnel. The dam of Nanhua Reservoir is a central zone divided by a rolling

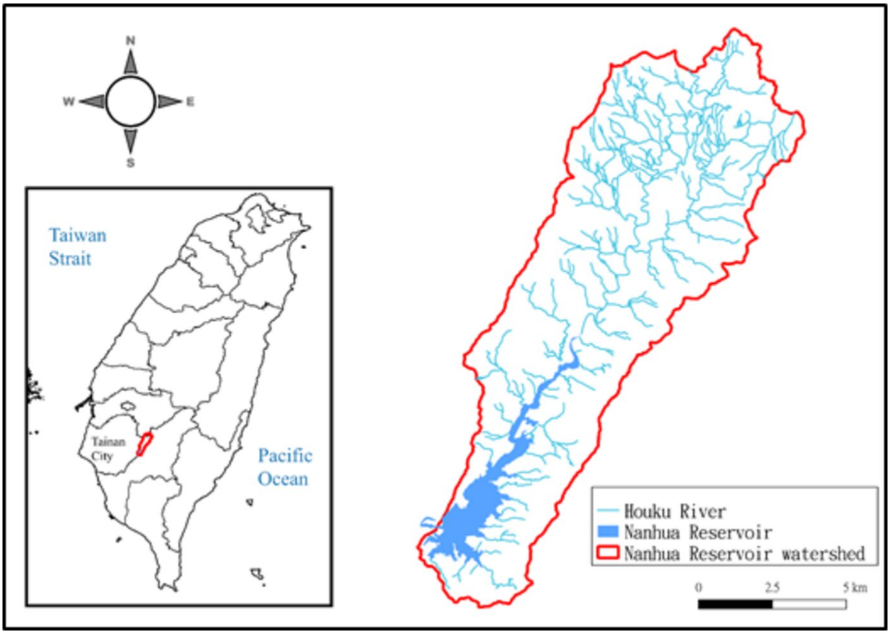

Fig. 1 Nanhua Reservoir location and watershed scope

earth-rock dam with a top elevation of 187.5 m and a fnnnnull water elevation of 180 m. The spillway was designed as a no-gate U-shaped free-flow weir with a top elevation of 180 m. The water intake was designed as an inclined tower type, with four ports at elevations of 170, 157, 144, and 131 m.

After several typhoon events over many years, Nanhua Reservoir has experienced severe sedimentation. As of October 2012, the capacity was only 99.43 million m (Anari et al. 2020), approximately 63% of the original design capacity. Therefore 2011, Nanhua Reservoir planned to build a Desilting tunnel, with construction starting in 2015. It took six years to complete and officially began operation in 2021. The structure of the Desilting tunnel mainly consists of a water entrance, shaft, gate, tunnel, and energy dissipation outlet. The water entrance is a rectangular cross-section of 15 m wide and 9.5 m high, with a flow area of 142.5 m (Amini et al. 2017). The Desilting tunnel is designed for a discharge of $1000m^3/s$, with a diameter of 9.5 m. The outlet connects to the original river channel of the Houku River for energy dissipation.

However, from 2021 to 2024, only one operated recorded during Typhoon Luipit in 2022 due to the lack of information from the original free overflow operation to varied options of hydraulic desiltaion selections, such as downstream replenishment sediment flushing, sluicing operation using Desilting tunnel and flood reduction control. Therefore, the reservoir capacity (Taiwan Water Corporation Sixth Branch 2023a) was still reduced from 89.35 million m (Anari et al. 2020) in 2021 to 89.20 million m (Anari et al. 2020) in 2023. we adopted a 2D numerical model to analyze the four hydraulic desolation scenarios mentioned and provide valuable desilting timing and efficiency for the decision-making for desilting operations in Nanhua Reservoir during typhoon events.

2.2 2-D Numerical Methodology

Two-dimensional (2D) models are invaluable for reservoir and water managers, providing detailed topographies and flow feature simulations. The Sedimentation and River Hydraulics (SRH-2D) model is particularly effective for describing two-dimensional hydraulic and sediment transport processes (Wang et al. 2020; Huang et al. 2019). This model can simulate a wide range of flow conditions—steady, quasi-steady, or unsteady—and sediment transport in cohesive and non-cohesive states. It also offers options for multi-size sediment transport with bed sorting and armoring (Lai 2010).

Lai et al. (2015) later developed a 2D layer-averaged turbidity current model, particularly suited for reservoir turbidity current simulations, which was applied in field cases by Huang et al. (2019) and Hung et al. (2022). The SRH-2D model is a powerful tool for simulating sediment transport; however, it has some limitations, particularly in predicting depth variations in sediment behavior. As a result, this model cannot simulate depth-dependent temperature effects, stratified sediment concentration, or the plunging mechanism of turbidity current. However, the transport velocity and cumulative outflow sediment load can be well evaluated after model verification by incorporating specific modifications related to entrainment effects, gravity differences, and outflow discharge in the conservation and momentum equations. The behavior of fine sediments in complex flows can be effectively simulated in a reservoir, as demonstrated by Wang et al. (2020), and Huang (2024). The model solves hydraulic mechanisms using mass conservation and momentum equations (as shown in Eq. 1 to 3) and simulates turbidity current transport using non-equilibrium sediment transport equations (as shown in Eqs. 4 and 5). Detailed numerical methods are described by Lai et al. (2015) and Huang et al. (2019).

$$\frac{\partial h_t}{\partial t} + \frac{\partial h_t U}{\partial x} + \frac{\partial h_t V}{\partial y} = e_w U_{av} \tag{1}$$

$$\frac{\partial h_t U}{\partial t} + \frac{\partial h_t UU}{\partial x} + \frac{\partial h_t VU}{\partial y} = \frac{\partial h_t T_{txx}}{\partial x} + \frac{\partial h_t T_{txy}}{\partial y} - (RgC_t)\, h_t \frac{\partial Z_t}{\partial x} - \frac{Rg}{2} h_t^2 \frac{\partial C_t}{\partial x} - (1 + r_w)\, \frac{\tau_{dx}}{\rho_s} \tag{2}$$

$$\frac{\partial h_t V}{\partial t} + \frac{\partial h_t UV}{\partial x} + \frac{\partial h_t VV}{\partial y} = \frac{\partial h T_{txy}}{\partial x} + \frac{\partial h T_{tyy}}{\partial y} - (RgC_t)\, h_t \frac{\partial Z_t}{\partial y} - \frac{Rg}{2} h_t^2 \frac{\partial C_t}{\partial y} - (1 + r_w)\, \frac{\tau_{dy}}{\rho_s} \tag{3}$$

$$\frac{\partial h_t C_{kt}}{\partial t} + \frac{\partial h_t U C_{kt}}{\partial x} + \frac{\partial h_t V C_{kt}}{\partial y} = w_{kt}\left(p_{kt} E_{kt} - C_{bk}\right) \tag{4}$$

$$(1 - \gamma_b)\, \frac{\partial Z_{bt}}{\partial t} = -\sum\nolimits_k w_{kt}\left(p_{kt} E_{kt} - C_{bk}\right) \tag{5}$$

Where, h_t: turbidity current thickness; t: time; x and y: x- and y-direction in Cartesian coordinates; U and V: velocity in the x- and y-directions; U_{av}: average velocity defined as $\sqrt{U^2 + V^2}$; e_w: dimensionless entrainment coefficient; T_{txx}, T_{txy}, T_{tyy}: dispersion terms; R: specific gravity of sediment in the turbidity current (R = $s - 1$ and $s = \frac{\rho_D}{\rho_w}$); ρ_D: density of sediment; ρ_w: density of ambient water; g: acceleration of gravity; C_t: total suspended sediment concentration; Z_t: turbidity current top elevation; r_w: friction between upper ambient water and the bottom turbidity current; ρ_s: mixture density; τ_{dx} and τ_{dy}: bed shear stresses in x - and y - direction; C_{kt}: layer-averaged volumetric concentration of the k_{th} sediment size class; w_{kt}: fall velocity of the k_{th} sediment size class; p_{kt}: volume fraction of the k_{th} sediment size class; E_{kt}: erosion rate potential; C_{bk}: near-bed concentration of the k_{th} size class; γ_b: porosity of bed sediment; Z_{bt}: bed elevation.

e_w = dimensionless entrainment coefficient; It is computed according to the expression developed by Lai et al. (Parker et al. 1987; Lai et al. 2015):

$$e_w = m_e \frac{0.075}{\sqrt{1 + 718 R_i^{2.4}}} \tag{6}$$

$$R_i = \frac{g h_p R C_t}{{U_{ap}}^2} \tag{7}$$

Where m_e = multiplier factor used as a numerical calibration parameter. In this study, 1.0 is used unless it is stated otherwise. R_i = bulk Richardson number (Toniolo et al. 2007); h_p = water depth at plunging point location; U_{ap} = average velocity at plunging point location.

r_w terms in Eqs. (2) and (3) represent the interfacial drag between upper ambient water and the current. The total drag components in the x and y directions are computed as follows:

$$(1 + r_w)(\tau_{dx}, \tau_{dy}) = \rho C_f \sqrt{U^2 + V^2}\,(U, V) \tag{8}$$

Where C_f = total drag coefficient combining both bed and interfacial drags, in Eqs. (2) and (3) T_{txx}, T_{txy}, T_{tyy} are the layer-averaged turbulence and dispersive stresses, formulations as follows (Lai 2010):

$$T_{txx} = 2(\upsilon + \upsilon_t)\frac{\partial U}{\partial x} \tag{9}$$

$$T_{tyy} = 2(\upsilon + \upsilon_t)\frac{\partial V}{\partial y} \tag{10}$$

$$T_{txy} = (\upsilon + \upsilon_t)\left(\frac{\partial U}{\partial y} + \frac{\partial V}{\partial x}\right) \tag{11}$$

Equations (8), (9), and (10) are calculated with Boussinesq formulation (Lai and Greimann, 2010), where υ = kinematic viscosity of the mixture; υ_t = eddy viscosity due to turbulence and dispersion. A turbulence model, a depth-averaged parabolic model, was used to calculate the turbulent eddy viscosity. The equation of the parabolic model is shown in Eq. (11):

$$\upsilon_t = a_t V_* h_t \tag{12}$$

Where a_t = constant and ranges from 0.05–1.0; V_* = bed frictional velocity, $V_* = \left(\sqrt{\tau_{dx}^2 + \tau_{dy}^2}/\rho\right)^{0.5}$。

The layer-averaged concentration is used to calculate the near-bed concentration (C_{bk}). The relationship between C_{bk} and the shape factor of sediment particle r_{0k} is $C_{bk} = r_{0k} C_k$ (García, 1994), and the shape factor is computed by:

$$r_{0k} = 1.64 + 0.4\left(\frac{d_k}{d_{gm}}\right)^{1.64}; \quad \ln\left(d_{gm}\right) = \frac{\Sigma\ C_{kt}\ ln(d_k)}{\Sigma\ C_k} \tag{13}$$

Where d_k = diameter of sediment size k;d_{gm} = the geometric mean diameter, The erosional rate potential (E_{kt}) is based on the equation of Engelund and Hansen (Engelund and Hansen, 1972). It is widely used in streams and reservoirs for fine sediment transport and is suitable for field-scale applications, it may be expressed as:

$$E_{kt} = 0.05 m_E \frac{\sqrt{U^2 + V^2}}{h_t\sqrt{\frac{(s-1)g}{d_k}}}\left[\frac{V_*^2}{(s-1)\,g d_k}\right]^{1.5} \tag{14}$$

When suspended sediment flows, deposition or erosion occurs as the concentration approaches equilibrium. The SRH-2D model uses two adaptation coefficients—the deposition and the erosion coefficients—to simulate this process, ensuring the accurate representation of suspended sediment transport and concentration equilibrium. In the SRH-2D mobile bed model, the governing equations for achieving sediment concentration equilibrium during deposition or erosion are calculated as follows:

$$S_e = \frac{q_s^* - q_s}{L_s} \tag{15}$$

$$L_s = \frac{\lambda\, U_{av} h_l}{w_{kt}} \tag{16}$$

Where S_e = unit sediment equilibrium transport rate; q_s^* = local sediment transport capacity; q_s = sediment transport flux advected into the local area from upstream; L_s = distance of suspended sediment transport, known as adaptation length; λ = user-specified parameter for net deposition and erosion. Default values for the two adaptation coefficients are 0.25 and 1.0 for deposition and erosion, respectively. h_l = local water depth.

2.3 Boundary Conditions

The preprocessing steps of the numerical model involved handling numerical terrain data and preparing the 2D simulation grid file required for SRH-2D simulations using SMS software (Surface-water Modeling System, v.13.0). The 2D simulation range extends from the upstream Guanshan No. 9 Bridge in the reservoir area (Sect. 48) to the area at the dam site. The inflow boundary is set at Guanshan No. 9 Bridge, and the downstream outflow boundaries include the Desilting tunnel (DT) outflow, the spillway (SW) free overflow, and the water intake (elevation 151 m). The grid density in the reservoir area refers to the suggestion of Hung et al. (2022) and is set in the 40–50 m range. The time step and the number of simulated grids are between 0.1 and 1.0 (sec) and less than 20,000, respectively. Inverse distance weighting (IDW) was used to interpolate terrain elevations for empty areas within each grid cell based on known numerical elevation data for the reservoir area. Manning's roughness coefficient refers to the grain size (as shown in Table 1) and is set to 0.006. The grain size distribution was based on suspended load sampling results at Guanshan No. 9

Bridge (Taiwan Water Corporation Sixth Branch 2021), as shown in Table 1. The detailed 2D numerical model setup for Nanhua Reservoir, including terrain elevations, boundary conditions, and key sediment observation points in the reservoir area, is illustrated in Fig. 2.

Based on the field measurement during Typhoon Lupit in 2021 (Taiwan Water Corporation Sixth Branch 2021), the suspended sediment concentration could be related to the inflow discharge as the following regression formula.

$$Q_s = aQ^m = 11.30Q^{1.89}, \quad \mathrm{R}^2 = 0.90 \tag{17}$$

where a and m are the coefficients of the regression relationship; Q_s is inflow sediment discharge (ton/day); Q is inflow discharge (m^3/s).

2.4 Study Cases

The Nanhua Reservoir was initially designed with a free overflow spillway without gate control for discharge. Apart from the spillway in front of the dam and the Desilting tunnel on the right bank of the reservoir's middle part, there are no other flood discharge and bottom outlet desilting facilities to aid hydraulic desilting. This gradually reduces the reservoir's capacity if the desilting operation is poorly implemented. To enhance the effectiveness of hydraulic desilting without affecting the reservoir's water storage and supply functions, it is crucial to analyze and improve the current water discharge facilities to balance sediment inflow and outflow in the reservoir.

Based on the operational experience during Typhoon Lupit in 2021 (as shown in Table 2), although the measurement location of Sect. 13 near the entrance of the desilting tunnel observed a high sediment concentration of over 10,000 PPM, the concentration measured at the tunnel's discharge point significantly decreased. This can be attributed to the following factors. The reservoir water level exceeded 180 m then, causing the free overflow in front of the dam to direct the sediment-laden flow towards the downstream dam. The desilting tunnel was not fully open, limiting the influence of the pressure flow field. After the water flow passed the measurement location of Sect. 13, the cross-section of the reservoir widened, leading to the diffusion and dilution of the sediment concentration. The slope of the reservoir area upstream of the desilting tunnel entrance has changed from the original design, causing the main flow of high sediment concentration observed by the measurement location of Sect. 13 to shift towards the central cross-section of the reservoir. As a result, only a portion of the sediment is discharged through the desilting tunnel.

In terms of regulating reservoir operation strategies, this study utilizes a validated two-dimensional numerical model (as described in the previous section) to develop different water release strategies based on various operational goals. These strategies include high, medium, and low initial water levels or operation strategies focused on " free overflow," "replenishment sediment flushing," " sluicing operation," and flood reduction. The effectiveness of hydraulic desiltation under different operational strategies is tested through simulations. The historical typhoon flood event used for this study is the 2021 Typhoon Lupit. Using the operational optimization model (Taiwan Water Corporation Sixth Branch 2023b),

Table 1 Particle size at Guanshan no. 9 Bridge

Diameter Distribution	D_{10}	D_{20}	D_{30}	D_{40}	D_{50}	D_{65}	D_{75}	D_{90}	D_{100}
Grain size (mm)	0.0130	0.0532	0.0750	0.0860	0.0932	0.1416	0.2151	0.3606	1.2409

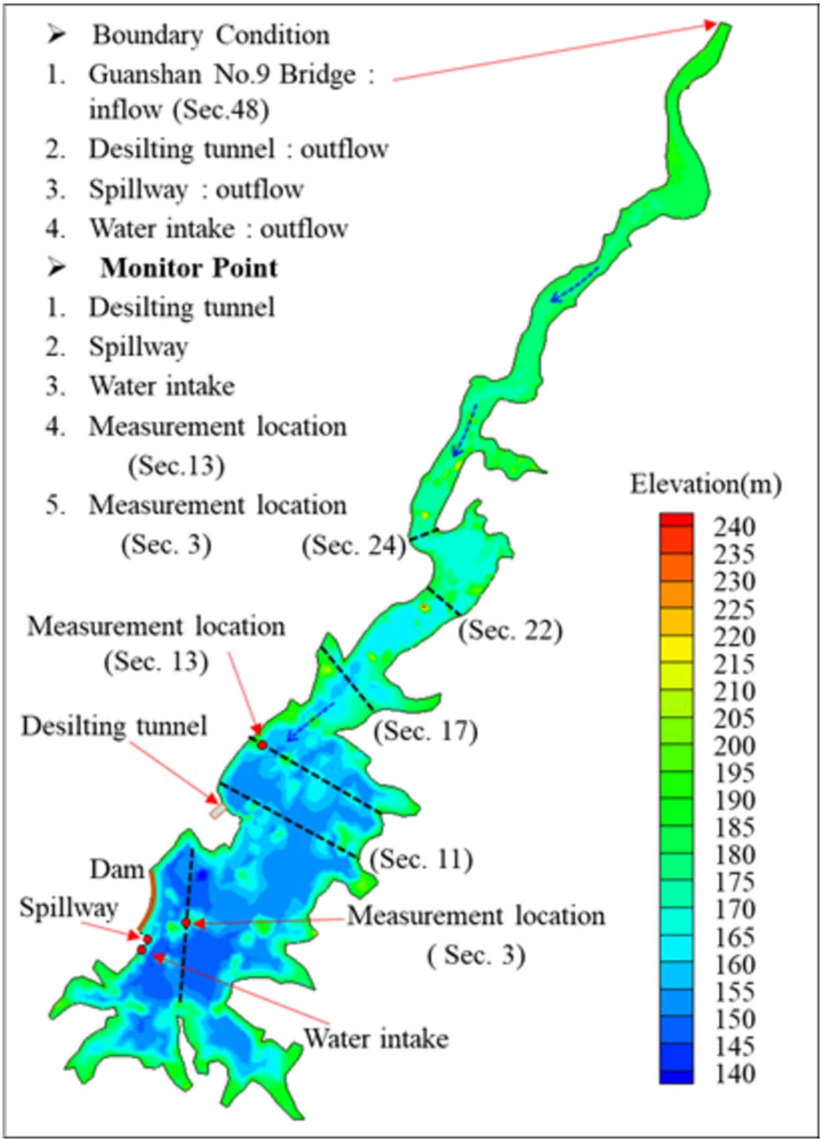

Fig. 2 Boundaries and measurement locations

Table 2 Typical event for model calibration and desilting efficiency assessment

Events	Year	Total precipitation (mm)	Rainfall intensity (mm/hr)	Inflow volume (10^6 m^3)	Peak inflow discharge (m^3/s)	Initial water level (m)	Max outflow discharge (m^3/s)
Typhoon Lupit	2021	731	34.0	68.8	812	180.22	436

the reservoir water levels and discharge flow rates through different facilities were determined for the four mentioned operational strategies. The initial reservoir water levels were assumed to be 175.5, 177.5, and 180.5 m. Based on the combination of the aforementioned operational strategies, typhoon events, and initial reservoir water levels, this study designs scenarios for different operation strategies of the Nanhua Reservoir. These scenarios include peak inflow rates, peak sediment inflow rates, and case analyses, as listed in Table 3. Each operational strategy includes three initial reservoir water levels, resulting in 12 reservoir operation strategy simulation scenarios. The boundary conditions for the four reservoir operation strategies are designed based on the inflow hydrograph of Typhoon Lupit. The inflow and outflow boundary conditions are shown in Fig. 3, and the essential contents of the four operation strategy scenarios are as follows:

(1) In the “free overflow” simulation scenario, the Desilting tunnel remains closed without releasing water. Free overflow begins at the spillway in the 71st hour of the simulation and continues until the end. The peak discharge rate is 414 m^3/s, with a constant water intake of 12 m^3/s at the water intake.
(2) In the downstream “replenishment sediment flushing” simulation scenario, the Desilting tunnel is opened in the 55th hour of the simulation, discharging 100 m^3/s. From the 56th to the 96th hour, the discharge rate is increased to 300 m^3/s, with a constant water intake of 12 m^3/s.
(3) In the “sluicing operation” simulation scenario, the Desilting tunnel is opened in the 2nd hour, maintaining a discharge rate of 50 m^3/s. From the 75th to the 77th hour, the discharge rate is increased to 300 m^3/s. From the 78th to the 83rd hour, the discharge rate is increased to 550 m^3/s. From the 107th to the 108th hour, the discharge rate is further increased to 800 m^3/s, with a constant water intake of 12 m^3/s.
(4) In the “flood reduction” simulation scenario, the Desilting tunnel entrance is opened from the 21st to the 116th hour of the simulation, discharging 100 to 150 m^3/s. The constant water intake at the intake tower is 12 m^3/s.

Table 3 Scenarios of four reservoir operation strategies

Cases	Operation condition	Initial water level (m)	Cases	Operation condition	Initial water level (m)	Cases	Operation condition	Initial water level (m)
1	Free overflow	175.5	5	Free overflow	177.5	9	Free overflow	180.5
2	Replenishment sediment flushing		6	Replenishment sediment flushing		10	Replenishment sediment flushing	
3	Sluicing operation		7	Sluicing operation		11	Sluicing operation	
4	Flood reduction		8	Flood reduction		12	Flood reduction	

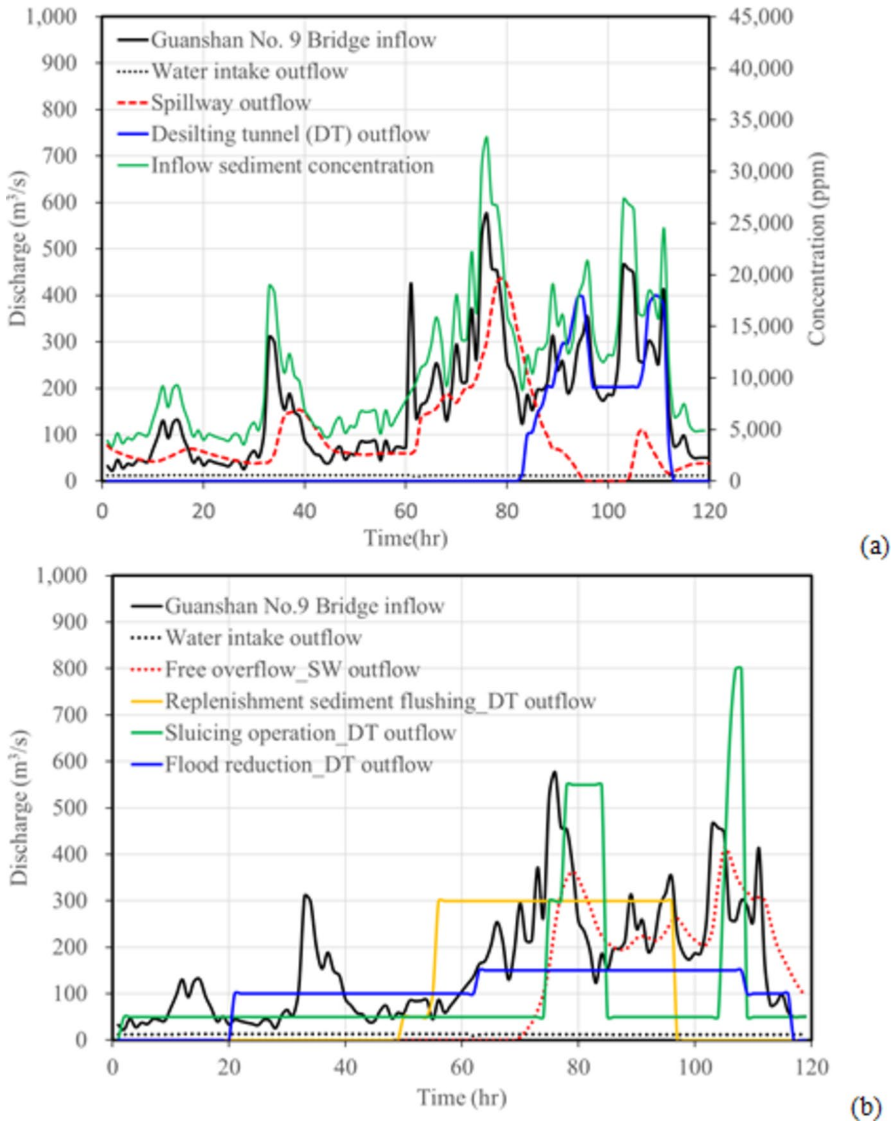

Fig. 3 Boundary conditions of (**a**) Typhoon Lupit (**b**) four reservoir operation strategies

3 Result and Discussion

3.1 Model Calibration and Verification

In this project, the two-dimensional numerical model for the Nanhua Reservoir was validated using actual observed or operational data during Typhoon Lupit in 2021. This included inflow into the reservoir, discharge from the Desilting tunnel, spillway discharge, and outflow from the water intake. Sediment transport within the reservoir was calculated

Table 4 Parameters of numerical simulation

Parameters	Time step dt (hr)	Manning *n* value	Sediment transport equation	Turbulence coefficient C_μ	Deposition coefficient Adept	Erosion coefficient A_{ero}
Values	0.1	0.006	Engelandn-Hansen (1972)	0.7	0.25	1.0

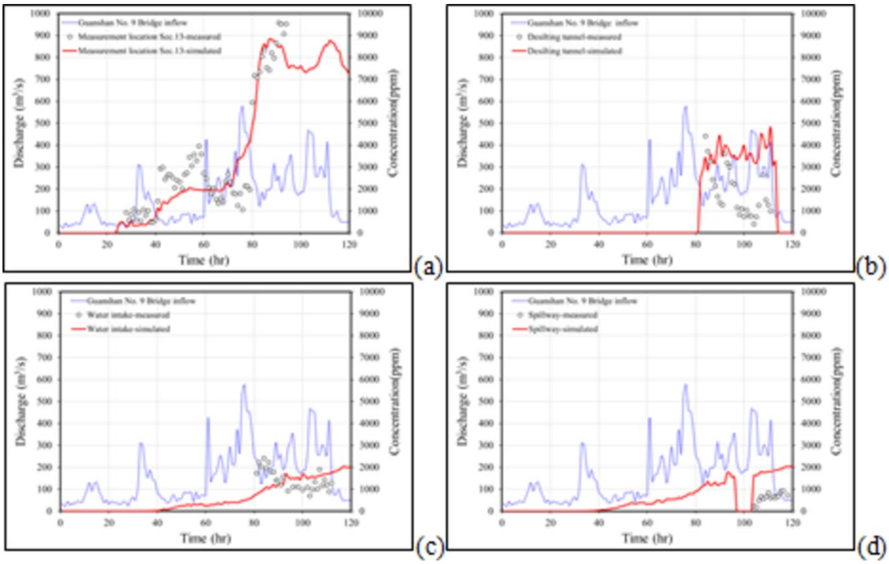

Fig. 4 Numerical model calibration using Typhoon Lupit (**a**) Sect. 13 (**b**) DT (**c**) water intake (**d**) spillway

using the Parker formula (1990). The hydrological hydrographs for the inflow and outflow boundary conditions are shown in Fig. 3(a), representing the actual operational process and observed concentration hydrographs. The model calibration was based on the measured outflow sediment concentration during this event, and the 2DLAM model recorded and output the sediment concentration hydrographs at the Desilting tunnel and the water intake during the turbidity current simulation.

The parameters for the two-dimensional simulation and validation of the Nanhua Reservoir are listed in Table 4. The validation results for the measurement location and outflows are shown in Fig. 4. The time difference between the upstream inflow peak and the downstream outflow sediment concentration peak allows an approximate estimation of the time required for sediment transport from the upstream inflow to the measurement locations and outflow facilities. Figure 4 shows that the sediment concentration peaks reach the measurement location Sect. 13 at about the 80th hour later, the desilting tunnel entrance at about the 83rd hour, and the water intake entrance at about the 89th hour. Comparing the observed and simulated sediment concentration values at various points reveals that, despite differences in sediment concentration values and delay times, the overall trend and movement of sediment concentration are generally consistent.

Additionally, this study collected data on the sediment load from the Desilting tunnel, calculated the cumulative sediment load and sediment desilting efficiency (=total outflow

Table 5 Numerical model calibration and verification

Events	Data	Inflow Peak discharge (m^3/s)	Inflow Peak sediment discharge (ton/s)	Inflow sediment load (tons)	Outflow sediment load at DT (tons)	Desilting efficiency (%)	Error (%)
Typhoon Lupit	Measured	577	19.22	1,115,490	65,005	5.83	1.63
	Simulated				83,182	7.46	
Typhoon Kalmaegi	Physical model	2,545	355.26	7,292,774	1,769,510	24.26	0.63
	Simulated				1,815,412	24.89	
25-year return period flood	Physical model	1,622	145.57	5,377,424	1,403,275	26.10	−1.01
	Simulated				1,349,147	25.09	

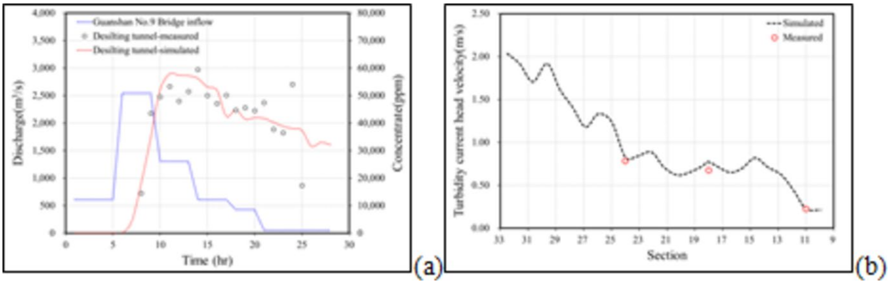

Fig. 5 Numerical model verification using Typhoon Kalmaegi (**a**) outflow concentration at DT (**b**) head velocity

sediment load/ total inflow sediment load), and compared these with the simulation results in Table 5. The cumulative outflow sediment load was 65,005 tons, with a desilting efficiency of approximately 5.83%. The simulated outflow sediment load was 83,182 tons, with a desilting efficiency of roughly 7.46%. The related error (= (simulated-measured)/ measures) is about 1.63%.

After completing the calibration simulation using data from Typhoon Lupit, the verification case utilized boundary conditions from the 2008 Typhoon Kalmaegi and a 25-year return period flood event, as tested in the Nanhua Reservoir model experiment (Southern Region Water Resources Office, 2014). These boundary conditions were applied to the two-dimensional numerical model for verification using model parameters validated during calibration. The hydrological and sediment hydrographs for the inflow and outflow boundary conditions of Typhoon Kalmaegi and the 25-year return period event were compared with numerical model results.

The verification results for the sediment prevention tunnel in the Nanhua Reservoir's two-dimensional simulation are presented, including the sediment concentration distribution at the tunnel entrance (Figs. 5(a) and 6(a)). Additionally, data on the head movement speed of density currents were collected from Typhoon Kalmaegi and 25-year return period flood model experiments. Cross-Sects. 24, 17, and 11, representing upstream, midstream, and the area near the tunnel entrance, were selected for comparison (Figs. 5(b) and 6(b)).

For the Typhoon Kalmaegi verification case, the sediment discharge volume was 1,815,412 tons, with a sediment discharge ratio of 24.89%. The 25-year return period event

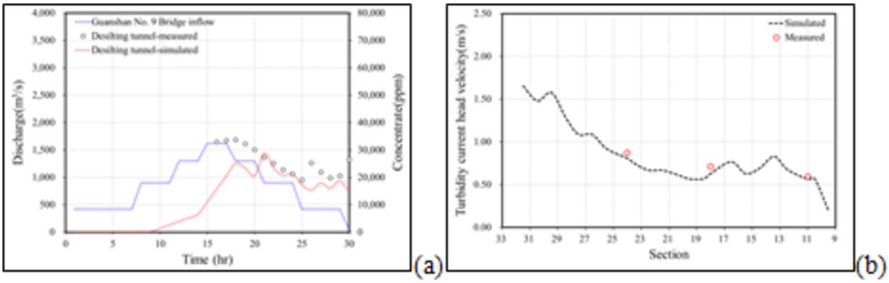

Fig. 6 Numerical model verification using Q 25 event (**a**) outflow concentration at DT (**b**) head velocity

yielded a sediment discharge volume of 1,349,147 tons, with a sediment discharge ratio of 25.09%. The calculated outflow sediment load and desilting efficiency are listed in Table 5. The validation and verification results indicate that while there are minor discrepancies in hourly sediment concentration between measured and simulated values, the simulated outflow sediment load closely aligns with the measured data.

The errors between measured and simulated outflow sediment load for Typhoon Lupit, Typhoon Kalmaegi, and the 25-year return period event were 1.63%, 0.63%, and −1.01%, respectively. The average error of the head velocity of Typhoon Kalmaegi and the 25-year return period event was −0.5%. These findings are consistent with the work of Lai et al. (2015), Huang et al. (2019), and Hung et al. (2022), confirming the accuracy of the cumulative sediment discharge simulations.

Moreover, the simulated head movement speed of density currents along the reservoir's longitudinal direction matched the measured values from model experiments, demonstrating that the two-dimensional model of Nanhua Reservoir can effectively simulate density currents and high-concentration turbidity transport phenomena. The desilting efficiency from the sediment prevention tunnel in the two-dimensional model ranged from 7.46 to 25.09%, showing a positive correlation with inflow and sediment inflow volumes. These results offer valuable insights into sediment transport characteristics and sediment prevention operations within the reservoir.

3.2 Sediment Transportation Simulation

An initial reservoir water level of EL. 175.5 m is in the hydraulic sediment prevention operation. The two-dimensional sediment concentration distributions are shown for scenarios including free overflow (C-1), sluicing operation (C-2), replenishment sediment flushing (C-3), and flood reduction (C-4). These distributions, along with the sediment concentration and flow field distributions at cross-Sects. 13 and 22, are depicted in Fig. 7. The simulation shows that the concentration decreased significantly after Sect. 13 due to the geometric and bend effect. The different hydraulic sediment prevention operations will affect sediment transport velocity and distribution. This will result in different outflow sediment concentrations and outflow sediment loads during each hydraulic outlet operation. In all simulation cases, the inflow sediment concentration increases to its first peak (33,318 ppm), which is defined as an essential maximum inflow sediment value to discuss the concentration decreasing at different locations. The peak inflow sediment concentration at the Guanshan No. 9 Bridge is estimated at hour 0. Peak sediment concentrations and their correspond-

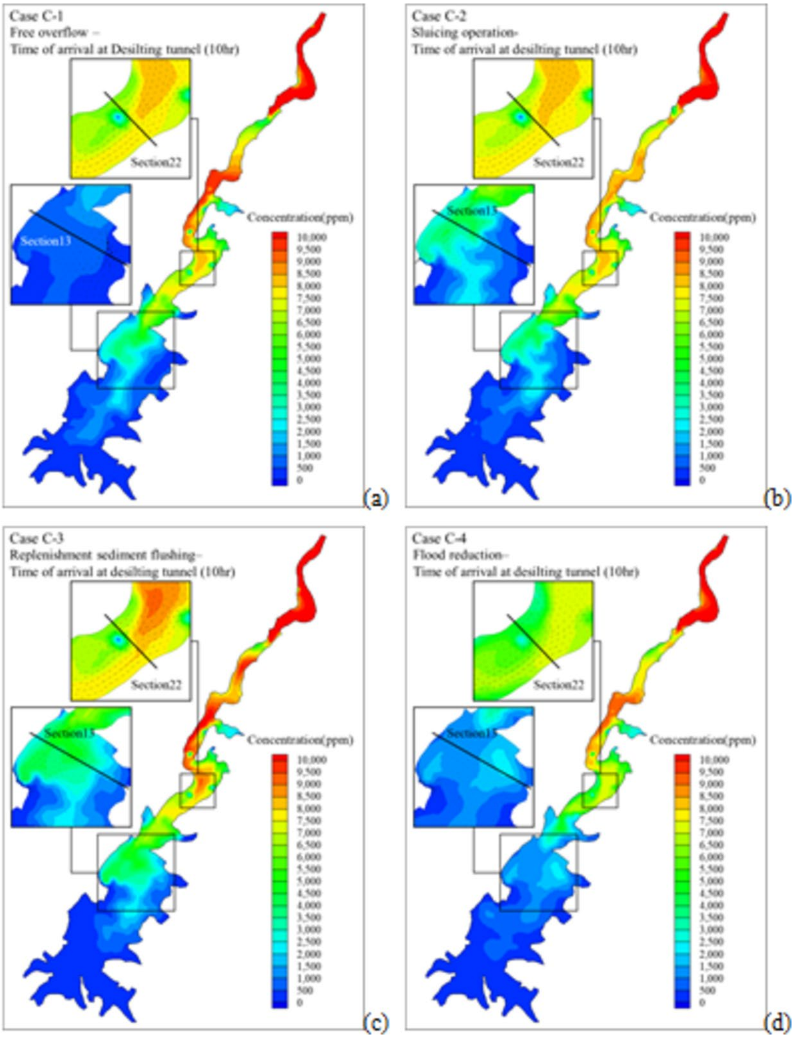

Fig. 7 Simulated concentration distribution at peak inflow (**a**) free overflow (**b**) sluicing operation (**c**) Replenishment sediment flushing (**d**) Flood reduction during Typhoon Lupit event

ing times at each monitoring location are listed in Table 6. These peak concentration data, categorized by monitoring location, are analyzed to understand the transport time and peak sediment relationship from the Guanshan No. 9 Bridge to each monitoring point, as shown in Fig. 2.

3.3 Discussions

To analyze the sediment transport characteristics in Nanhua Reservoir during flood periods, this study consolidates the inflow sediment load and the sediment discharge from the desilting tunnel and spillway for various hydraulic desilting scenarios. The sediment desilting

Table 6 Transportation time and concentration dilution

Events	Location	Transportation time(hour)	Peak concentration (ppm)
	Guanshan No.9 Bridge (Inflow boundary)	0	33,318
C-1	Measurement station (Sect. 13)	7	3816
	Desilting tunnel	10	2310
	Water intake	15	474
C-2	Measurement station (Sect. 13)	8	4722
	Desilting tunnel	10	3218
	Water intake	15	332
C-3	Measurement station (Sect. 13)	7	4906
	Desilting tunnel	10	3624
	Water intake	18	238
C-4	Measurement station (Sect. 13)	7	3013
	Desilting tunnel	11	1377
	Water intake	22	312
C-5	Measurement station (Sect. 13)	10	4106
	Desilting tunnel	13	2706
	Water intake	37	372
C-6	Measurement station (Sect. 13)	8	4786
	Desilting tunnel	19	4067
	Water intake	29	451
C-7	Measurement station (Sect. 13)	8	4294
	Desilting tunnel	12	3149
	Water intake	25	416
C-8	Measurement station (Sect. 13)	9	5373
	Desilting tunnel	14	4142
	Water intake	30	337
C-9	Measurement station (Sect. 13)	8	4219
	Desilting tunnel	15	2503
	Water intake	38	546
C-10	Measurement station (Sect. 13)	8	4606
	Desilting tunnel	20	3315
	Water intake	28	358
C-11	Measurement station (Sect. 13)	8	4606
	Desilting tunnel	12	3149
	Water intake	23	327
C-12	Measurement station (Sect. 13)	11	3572
	Desilting tunnel	13	2544
	Water intake	34	588

efficiency for each outlet structure is calculated accordingly. Additionally, the peak concentrations at Guanshan No. 9 Bridge, measurement location No. 13 in the reservoir, and the spillway during the simulation periods are summarized to calculate the percentage of peak concentrations at various locations relative to the peak sediment concentration at Guanshan No. 9 Bridge. The results for outflow sediment load, Desilting efficiency, and peak concentration ratio for each scenario are shown in Table 7, where ①, ②, ③, and ④ represent the peak sediment concentrations at Guanshan No. 9 Bridge, measurement location No. 13 in the reservoir, the desilting tunnel, and measurement location No. 3, respectively.

Table 7 Simulated hydraulic desiltation values

Event	Typhoon Lupit						
	Inflow sediment load (10^6ton)		1.09	Peak inflow concentration (ppm)			33,318
Cases	Outlets	Outflow sediment load (10^3 tons)	Desilting efficiency (%)	Cases	Outlets	Outflow sediment (10^3 tons)	Desilting efficiency (%)
C-1 (Initial water level EL. 175.5 m & Free overflow)	Desilting tunnel	0.00	0.00	C-7 (Initial water level EL. 177.5 m & Sluicing operation)	Desilting tunnel	61.1	5.59
	Spillway	10.8	0.99		Spillway	0.00	0.00
	Peak concentration ratio				Peak concentration ratio		
	②/①	③/①	④/①		②/①	③/①	④/①
	0.11	0.07	0.03		0.13	0.09	0.02
C-2 (Initial water level EL. 175.5 m & Replenishment sediment flushing)	Desilting tunnel	64.2	5.88	C-8 (Initial water level EL. 177.5 m & Flood reduction)	Desilting tunnel	45.7	4.18
	Spillway	0.00	0.00		Spillway	0.00	0.00
	Peak concentration ratio				Peak concentration ratio		
	②/①	③/①	④/①		②/①	③/①	④/①
	0.14	0.10	0.02		0.16	0.10	0.02
C-3 (Initial water level EL. 175.5 m & Sluicing operation)	Desilting tunnel	58.6	5.36	C-9 (Initial water level EL. 180.5 m & Free overflow)	Desilting tunnel	0.00	0.00
	Spillway	0.00	0.00		Spillway	13.4	1.22
	Peak concentration ratio				Peak concentration ratio		
	②/①	③/①	④/①		②/①	③/①	④/①
	0.15	0.11	0.04		0.13	0.08	0.02
C-4 (Initial water level EL. 175.5 m & Flood reduction)	Desilting tunnel	22.8	2.09	C-10 (Initial water level EL. 180.5 m & Replenishment sediment flushing)	Desilting tunnel	63.4	5.80
	Spillway	0.00	0.00		Spillway	0.00	0.00
	Peak concentration ratio				Peak concentration ratio		
	②/①	③/①	④/①		②/①	③/①	④/①
	0.09	0.04	0.02		0.14	0.10	0.02
C-5 (Initial water level EL. 177.5 m & Free overflow)	Desilting tunnel	0.00	0.00	C-11 (Initial water level EL. 180.5 m & Sluicing operation)	Desilting tunnel	43.5	3.99
	Spillway	7.5	0.69		Spillway	0.00	0.00
	Peak concentration ratio				Peak concentration ratio		
	②/①	③/①	④/①		②/①	③/①	④/①
	0.12	0.08	0.02		0.14	0.09	0.02
C-6 (Initial water level EL. 177.5 m & Replenishment sediment flushing)	Desilting tunnel	79.6	7.29	C-12 (Initial water level EL. 180.5 m & Flood reduction)	Desilting tunnel	40.2	3.68
	Spillway	0.00	0.00		Spillway	0.00	0.00
	Peak concentration ratio				Peak concentration ratio		
	②/①	③/①	④/①		②/①	③/①	④/①
	0.14	0.12	0.03		0.11	0.08	0.02

The four major operational strategies for hydraulic desilting scenarios in Nanhua Reservoir, designed based on historical typhoon and flood events (free overflow, replenishment sediment flushing, sluicing operation, and flood reduction), were observed through two-dimensional numerical simulation results. The sediment concentration and flow field distribution at specific moments (such as peak flow and arrival at the desilting tunnel entrance) and specific locations (such as measurement location No. 13 in the reservoir and the spillway entrance) during typhoon and flood events were examined in Fig. 7. The results show that, under the total sediment inflow of 1.09×10^6 tons during Typhoon Lupit, the sediment discharge from the spillway in the free overflow scenario ranged between 7.5×10^3 and 13.4×10^3 tons. For the replenishment sediment flushing, sluicing operation, and flood reduction scenarios, the outflow sediment load from the desilting tunnel ranged from 63.4×10^3 tons to 79.6×10^3 tons, 43.5×10^3 tons to 61.1×10^3 tons, and 22.8×10^3 tons to 45.7×10^3 tons, respectively. The average peak concentration at the desilting tunnel entrance was approximately 3,009 ppm.

In the free overflow scenario, the sediment desilting efficiency of the spillway ranges from 0.69 to 1.22%, while the sediment desilting efficiency of the desilting tunnel is 0% due to its closure. The peak sediment concentration ratio between measurement location No. 13 in the reservoir and Guanshan No. 9 Bridge (②/①) ranges from 0.11 to 0.13. The peak sediment concentration ratio between the desilting tunnel and Guanshan No. 9 Bridge (③/①) ranges from 0.07 to 0.08, and the ratio between measurement location No. 3 and Guanshan No. 9 Bridge (④/①) ranges from 0.02 to 0.03.

In the replenishment sediment flushing, the sediment desilting efficiency of the desilting tunnel ranges from 5.80 to 7.29%. In comparison, the sediment desilting efficiency of the spillway is 0% due to the absence of overflow. The peak sediment concentration ratio between measurement location No. 13 in the reservoir and Guanshan No. 9 Bridge (②/①) is around 0.14. The peak sediment concentration ratio between the Desilting tunnel entrance and Guanshan No. 9 Bridge (③/①) ranges from 0.10 to 0.12, and the ratio between measurement location No. 3 and Guanshan No. 9 Bridge (④/①) ranges from 0.02 to 0.03.

In the sluicing operation scenario, the sediment desilting efficiency of the desilting tunnel ranges from 3.99 to 5.59%. In comparison, the sediment desilting efficiency of the spillway is 0% due to the absence of overflow. The peak sediment concentration ratio between measurement location No. 13 in the reservoir and Guanshan No. 9 Bridge (②/①) ranges from 0.13 to 0.15. The peak sediment concentration ratio between the desilting tunnel and Guanshan No. 9 Bridge (③/①) ranges from 0.09 to 0.11, and the ratio between the measurement location No. 3 and Guanshan No. 9 Bridge (④/①) ranges from 0.02 to 0.04.

In the flood reduction scenario, the sediment desilting efficiency of the desilting tunnel ranges from 2.09 to 4.18%. In comparison, the sediment desilting efficiency of the spillway is 0% due to the absence of overflow. The peak sediment concentration ratio between measurement location No. 13 in the reservoir and Guanshan No. 9 Bridge (②/①) ranges from 0.09 to 0.16. The peak sediment concentration ratio between the desilting tunnel and Guanshan No. 9 Bridge (③/①) ranges from 0.04 to 0.10, and the ratio between measurement location No. 3 and Guanshan No. 9 Bridge (④/①) is 0.02.

In this study, which focuses on multiple flood peak hydrographs and medium to high peak inflow (>700 m^3/s) events such as Typhoon Lupit, the maximum sediment desilting efficiency for the spillway in the free overflow scenario is approximately 1.22%. In the replenishment sediment flushing scenario, the maximum sediment desilting efficiency for the desilting tunnel is 7.29%. For the sluicing operation and flood reduction scenarios, the maximum sediment desilting efficiency for the desilting tunnel is 5.59% and 4.18%, respectively. The peak sediment concentration at Guanshan No. 9 Bridge reduces to about 13% at measurement location No. 13 in the reservoir, about 9% at the desilting tunnel, and about 2% in front of the dam (measurement location No. 3).

Table 8 Integrated results of transportation time, desilting efficiency, and peak concentration ratio

Scenarios	Free overflow	Replenishment sediment flushing	Sluicing operation	Flood reduction
Transportation time at DT	10 ~ 15	10 ~ 12	10 ~ 12	11 ~ 14
Desilting efficiency (at DT or SW)	0.69 ~ 1.22 (SW)	5.80 ~ 7.29 (DT)	3.99 ~ 5.59 (DT)	2.09 ~ 4.18 (DT)
Outflow discharge (10^6 m^3)	41.35	45.54	45.18	42.84
Peak concentration ratio at DT	0.07 ~ 0.08	0.10 ~ 0.12	0.09 ~ 0.11	0.04 ~ 0.10

4 Conclusions

The two-dimensional model of the Nanhua Reservoir established in this study was used to calibrate and validate model parameter settings through comparison with field observations and model test results. The sediment desilting efficiency for the validation cases of Typhoon Lupit, Typhoon Kalmaegi, and the 25-year return period flood were 7.46%, 24.89%, and 25.09%, respectively, with errors in the sediment discharge ratio ranging between −1.01% and 1.63%. This accurately reflects the phenomena of density currents or high-concentration turbidity transport in the field and the trend of cumulative sediment load at the outflow structures.

The simulated results of transportation time, desilting efficiency, and peak concentration ratio are integrated in Table 8. There is little difference in transportation time under the four hydraulic sediment prevention conditions. However, suppose a significant inflow of turbidity is discharged downstream from the sediment desilting tunnel located in the midstream section of Nanhua Reservoir for downstream replenishment sediment flushing. In that case, it will shorten the time it takes for the inflow turbidity to reach the dam site. Conversely, without sediment prevention operations by desilting tunnels, inflow turbidity will take longer to reach the dam site. The simulated desilting efficiency indicates that under conditions where the outflow volumes are roughly equal, the sediment desilting efficiency of the desilting tunnel is greater than that of the spillway. Furthermore, the sediment concentration ratio of the desilting tunnel is highest under replenishment sediment flushing, followed by sluicing operation, and flood reduction ranks third. This suggests that when the inflow turbidity reaches the desilting tunnel, immediate tunnel opening and higher discharge rates result in the most significant sediment discharge benefits. However, the peak concentration ratio shows little difference under the four hydraulic sediment prevention conditions. This is mainly due to the dilution effect of the reservoir water on the inflow turbidity, which is primarily related to the volume of the reservoir and the length of the inflow turbidity transport. The differences are insignificant since the two main factors affecting the peak concentration ratio are similar for these four scenarios.

Overall, the trend of decreasing sediment concentration during sediment transport in the reservoir can be observed from the peak concentration ratio. There is a certain degree of correlation between the peak sediment concentration at the Guanshan No. 9 Bridge inflow and the peak sediment concentration at measurement location 13 in the reservoir, the sediment desilting tunnel, and the intake tower entrance in front of the dam. Under lower flow conditions, due to slightly lower sediment discharge ratios and less apparent sediment transport phenomena, reservoir operation strategies may prioritize storage or regulated discharge based on reservoir water levels. However, under high flow conditions, replenishment sediment flushing and sluicing operation can achieve relatively better sediment prevention effects, especially when the inflow turbidity is about to reach the sediment desilting tunnel; timely opening of the sediment prevention tunnel and sufficient discharge rates can achieve optimal sediment prevention operations.

This study assesses desilting efficiency under four hydraulic sediment prevention operations, analyzing short-term effects using consistent hydrological inflow boundary conditions while varying outflow desilting strategies. Therefore, a model sensitivity analysis on factors such as sediment types, reservoir shapes, and water flow conditions is recommended for future research, as variations in these factors can significantly impact desilting efficiency and transport times. The long-term effects of sediment pattern change due to factors like catchment alterations and sediment accumulation are also critical areas for further investigation.

Acknowledgements The author acknowledges the Taiwan Water Corporation for providing the essential data for analysis and simulation. The author also wishes to thank the National Taiwan University and NCKU Research and Development Foundation for their workforce and technique support. In addition, the authors acknowledge the Technical Service Center, United States Bureau of Reclamation, for the numerical software provided for this study.

Author Contributions Fong-Zuo Lee developed the principal concepts, generated the analyzed data, and wrote the manuscript. Yu-Yun Du was responsible for the simulation of cases and framework editing.

Funding The Ministry of Science and Technology in Taiwan supported the presented study. The project numbers are NSTC 113-2221-E-005-027 and NSTC 113-2625-M-002-018.

Data Availability Not applicable.

Declarations

Ethical Approval Not applicable.

Consent To Participate Not applicable.

Consent To Publish Not applicable.

Competing Interests The authors declare that they have no conflict of interest in this work.

References

Afzalsoltani F, Yazdi J (2023) Development of a model for sediment evacuation from reservoirs. Environ Processes 10(3):46

Amini A, Venuleo S, Chamoun S, De Cesare G, Schleiss A, Takhtemina F (2017) Investigation of venting turbidity currents in the Rudbar-Lorestan reservoir in Iran. 85th Annual Meeting of International Commission on Large Dams, Prague, Czech Republic. 3-7 July 2017. https://infoscience.epfl.ch/record/229961?ln=en

Anari R, Hotchkiss RH, Langendoen EJ (2020) Elements for the successful computer simulation of sediment management strategies for reservoirs. Water 12(3):714

Annandale GW, Morris GL, Karki P (2016) Extending the life of reservoirs. Sustainable sediment management for dams and Run-of-River hydropower. The World Bank, Washington DC

Benicio SHM, Basso RE, Formiga KTM (2024) Global applications of the CE-QUAL-W2 model in reservoir eutrophication: a systematic review and perspectives for Brazil. Water 16(24):3556

Castro PW, Mantilla CA (2021) Implementation of strategies for the management of dams with sedimented reservoirs. Water Resour Manage 35(13):4399–4413

Chamoun S, De Cesare G, Schleiss AJ (2017) Management of turbidity current venting in reservoirs under different bed slopes. J Environ Manage 204:519–530
Chamoun S, De Cesare G, Schleiss AJ (2018) Influence of operational timing on the efficiency of venting turbidity currents. J Hydraul Eng 144(9):04018062
Chen SY (2020) Applying the two-dimensional (2D) layer-averaged turbidity current model to estimate outlet sediment concentration and desilting efficiency in the Zengwen Reservoir. Master thesis, National Taiwan University
De Cesare G, Schleiss A, Hermann F (2001) Impact of turbidity currents on reservoir sedimentation. J Hydraul Eng 127(1):6–16
De Cesare G, Boillat JL, Schleiss AJ (2006) Circulation in stratified lakes due to flood-induced turbidity currents. J Environ Eng 132(11):1508–1517
Engelund F, Hansen E (1972) A monograph on sediment transport in alluvial streams. Teknish Forlag, Technical, Copenhagen, Denmark
Garcia MH (1994) Depositional turbidity currents laden with poorly sorted sediment. J Hydraul Eng 120(11):1240–1263
Huang CC (2024) Navigating reservoir deposition challenges: evaluation of reservoir desilting strategy through a 4-stage life cycle assessment approach. Water Resour Manage 38:3937–3952
Huang CC, Lai YG, Lai JS, Tan YC (2019) Field and numerical modeling study of turbidity current in Shimen reservoir during typhoon events. J Hydraul Eng 145(5):05019003
Hung CC, Lai JS, Huang CC (2022) An efficient and economic desilitation strategy for reservoir sustainable development under the extreme flooding threaten. J Water Clim Change 13(3):1257–1274. https://doi.org/10.2166/wcc.2022.353
Imtiyaz N, Lee FZ, Lin GF, Lai JS (2024) Modeling and analysis of turbidity currents in a reservoir with the dredged guiding channel. KSCE J Civ Eng 28:3257–3269
Jodeau M, Chamoun S, Feng J, De Cesare G, Schleiss AJ (2018) Numerical modeling of turbidity currents with Ansys CFX and Telemac 3D. E3S Web of Conferences 40:03014. https://doi.org/10.1051/e3sconf/20184003014
Kalita HM (2020) A numerical model for 1d bed morphology calculations. Water Resour Manage 34(15):4975–4989
Lai YG (2010) Two-dimensional depth-averaged flow modeling with an unstructured hybrid mesh. J Hydraul Eng 136(1):12–23. https://doi.org/10.1061/(ASCE)HY.1943-7900.0000134
Lai YG, Greimann BP (2010) Predicting contraction scour with a two-dimensional depth-averaged model. J Hydraul Res 48(3):383–387
Lai YG, Huang JC, Wu KW (2015) Reservoir turbidity current modeling with a two-dimensional layer-averaged model. J Hydraul Eng 141(12). https://doi.org/10.1061/(ASCE)HY.1943-7900.0001041
Lee FZ, Huynh Nguyen NL (2024) Application of artificial countermeasures to enhance desilting efficiency in a reservoir under normal and extreme events. J Water Clim Change jwc2024632
Lee FZ, Lai JS, Tan YC, Sung CC (2014) Turbid density current venting through reservoir outlets. KSCE J Civ Eng 18(2):694–705. https://doi.org/10.1007/s12205-014-0275-y
Lee FZ, Liu CC, Lai JS, Chiueh PT (2023) Study on the application of Flushing channel with guide wall to reduce sedimentation in a reservoir. J Taiwan Agricultural Eng 69(2):11–21
Li T, Pasternack GB (2022) Water transfer redistributes sediment in small mountain reservoirs. Water Resour Manage 36(13):5033–5048
Morris GL, Fan J (2010) Reservoir sedimentation handbook. McGraw-Hill Book Co., New York. Ver. 1.04
Oehy CD, Schleiss AJ (2007) Control of turbidity currents in reservoirs by solid and permeable Obstacles. J Hydraul Eng 133(6):637–648
Parker G (1990) Surface-based bedload transport relation for gravel rivers. J Hydraul Res 28(4):417–436
Parker G, Garcia M, Fukushima Y, Yu W (1987) Experiments on turbidity currents over an erodible bed. J Hydraul Res 25(1):123–147
Sastre V, Loizeau JL, Greinert J, Naudts L, Arpagaus P, Anselmetti F, Wildi W (2010) Morphology and recent history of the Rhone river delta in lake Geneva (Switzerland). Swiss J Geosci 103:33–42
Schleiss AJ, Franca MJ, Juez C, De Cesare G (2016) Reservoir sedimentation. J Hydraul Res 54(6):595–614
Taiwan Water Corporation Sixth Branch (2021) Research on the establishment and application of a turbidity monitoring system for the Nanhua Reservoir inflow. Tainan (2021) Taiwan. (In Chinese)
Taiwan Water Corporation Sixth Branch (2023a) 2023 Nanhua Reservoir Sedimentation Survey. Tainan, Taiwan. (In Chinese)
Taiwan Water Corporation Sixth Branch (2023b) Nanhua Reservoir Operation Decision Support and Sediment Transport Monitoring. Tainan, Taiwan. (In Chinese)
Toniolo H, Parker G, Voller V (2007) Role of ponded turbidity currents in reservoir trap efficiency. J Hydraul Eng 133(6):579–595

Wang HW, Tsai BS, Hwang C, Chen GW, Kuo WC (2020) Efficiency of the drawdown Flushing and partition desilting of a reservoir in Taiwan. Water 12(8):2166

Ziaie R, Mohammadnezhad B, Taheriyoun M, Karimi A, Amiri S (2019) Evaluation of thermal stratification and eutrophication in Zayandeh Roud dam reservoir using Two-Dimensional CE-QUAL-W2 model. J Environ Eng 145(6):05019001

Zulfan J, Ginting B, Rimawan R (2023) Assessment of reservoir sedimentation and mitigation measures using 2D hydrodynamic modeling: Case study of Pandanduri Reservoir, Indonesia. IOP Conf. Ser.: Earth Environ Sci 1135(1):012018. https://doi.org/10.1088/1755-1315/1135/1/012018